Academic Education Publishing House

Industry Science and Engineering Vol. 2 No. 10, 2025

Lateral Error Simulation Analysis of Low-Frequency Large Displacement Standard Vibration Table

Hao Hou[1], Haolin Sun[2],*, Rilong Li[1]

[1] Beijing Great Wall Metrology & Test Technology Institute, AVIC, Beijing, China

[2] School of Mechatronical Engineering of Beijing Institute of Technology, Beijing, China

**Corresponding Author*

Abstract: This study addresses the lateral vibration error caused by the bending of guide rails under the gravitational load of the platform in the calibration technology of civil aircraft visual vibration measurement. We establish a systematic analysis method based on "simplified model theoretical derivation and validation through actual structure simulation." Simplification and modeling are performed using SolidWorks, while simulation analyses are conducted in Abaqus for various frequency conditions, covering the full frequency range from 0.1 Hz to 200 Hz (selecting 17 characteristic frequency points at 1/3 octave intervals). The focus is on quantifying the lateral displacement errors in the Y direction (perpendicular to the table surface) resulting from rail bending. The simulation results indicate that the maximum Y-direction displacement at the reference points of the vibration table surface is consistently on the order of 10^{-9} m, with corresponding maximum bending angles below 0.000002°. This error has a negligible effect on the Z-direction (table motion trajectory) vibration measurement results. This research provides a crucial error assessment basis for the calibration of visual vibration measurement systems, effectively supporting the advancement of noise field calibration techniques and offering a standardized simulation process for error analysis of similar high-precision vibration equipment.

Keywords: Low-Frequency Large Displacement Vibration Table; Lateral Error; Abaqus Simulation; Rail Bending; Civil Aircraft Vibration Calibration

1. Introduction

In the field of calibration for civil aircraft structures and aerodynamic noise fields, the calibration accuracy of visual vibration measurement systems directly determines the reliability of noise field evaluation results. The low-frequency large displacement standard vibration table serves as the core reference device for this calibration technology[1]. This vibration table must provide standard vibration excitation across a frequency range of 0.1 Hz to 200 Hz with a stroke of 0.5 m, allowing for the precision calibration of the visual vibration measurement system through comparisons with laser Doppler measurement results[2].

Currently, the low-frequency large displacement vibration table faces critical technical challenges in practical applications. Due to its large stroke (0.5 m) and unique motion characteristics at low frequencies, the guide rails are susceptible to bending deformation under the effects of platform gravity and dynamic loads, thereby introducing lateral vibration errors[3]. These errors exhibit a pattern where "the lower the frequency, the more significant the deviation." Without quantifying, evaluating, and correcting this issue, calibration deviations in the visual vibration measurement system could adversely affect the accuracy of noise field test data for civil aircraft. Existing studies predominantly focus on the dynamic design and control optimization of vibration tables[4], yet there is insufficient analysis on quantitatively assessing lateral errors caused by rail bending. A comprehensive simulation evaluation method that spans the entire frequency range is lacking, rendering it difficult to meet the strict requirements for error tracing in civil aircraft calibration projects.

To address this, this study is based on the design plan of the vibration table, as shown in Figure 1. We construct a refined simulation model that includes gravitational loads and motion constraints. Through simulation analysis under multiple frequency conditions, we quantify the magnitude and distribution of lateral errors and

validate their impact on measurement results. This provides theoretical support for calibration compensation in visual measurement systems, ensuring the reliability of noise field calibration technology for civil aircraft.

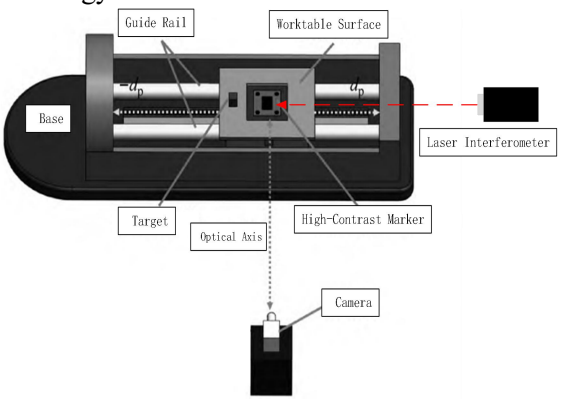

Figure 1. Schematic Diagram of Visual Vibration System Calibration Plan

2. Model Construction and Theoretical Foundation

2.1 Derivation of Simplified Model Theory

The core components of the vibration table consist of the table surface and guide rails. During operation, the table surface moves in a sinusoidal reciprocating motion along the guide rails, which concurrently bear three types of loads: a distributed load due to self-weight, concentrated gravitational loads from platform components, and a Z-direction torque induced by the driving forces (axial friction can be neglected). The force schematic is shown in Figure 2.

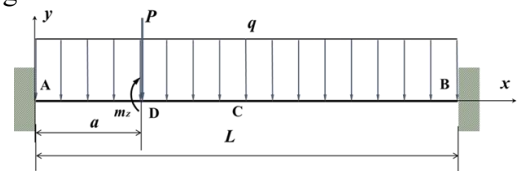

Figure 2. Force Schematic of the Guide Rails during Operation

Based on beam bending theory in materials mechanics, the bending angle \alpha of the guide rails (where the numerical values are minimal, thus sinα≈α and cosα≈1) results in an additional peak excitation acceleration $a_{p,G}$, expressed as:

$$a_{p,G} = g_{loc} \cdot \alpha \quad (1)$$

Where, g_{loc} represents the local gravitational acceleration (assumed to be 9.8m/s²).

The actual peak excitation acceleration $a_{p,actual}$ at the target point on the table surface arises from the combination of Z-direction ideal acceleration and lateral error acceleration, represented by:

$$a_{p,actual} = a_{p,E} \cdot \cos\alpha + g_{loc} \cdot \alpha \approx a_{p,E} + g_{loc} \cdot \alpha \quad (2)$$

In this equation, $a_{p,E}$ refers to the ideal Z-direction peak excitation acceleration.

The lateral error corresponding to deflection x(t) can be solved by double integrating the acceleration:

$$x(t) = \iint a\,(t)dt \quad (3)$$

The simplified model reveals an initial connection between guide rail bending and lateral error. However, it does not consider practical factors such as material properties and assembly gaps, necessitating further validation through detailed simulation.

2.2 Simplification of the Actual Structural Model and Introduction

To balance simulation accuracy with computational efficiency, we adopted a "retain key features - simplify non-essential details" modeling strategy. In SolidWorks, the assembly of the vibration table was optimized by removing features such as fillets and chamfers that do not affect the structural mechanical properties. Additionally, all units were standardized to the MKS system (meters, kilograms, seconds) to ensure compatibility with the Abaqus material library[5]. The simplified vibration table model is shown in Figure 3, with core components including the base (made of marble), table surface (marble plus side plates), magnetic base, and magnetic core. The design allows for a stroke of 0.5 m, with the motion speed curve following $v = A\sin(\omega t)$.

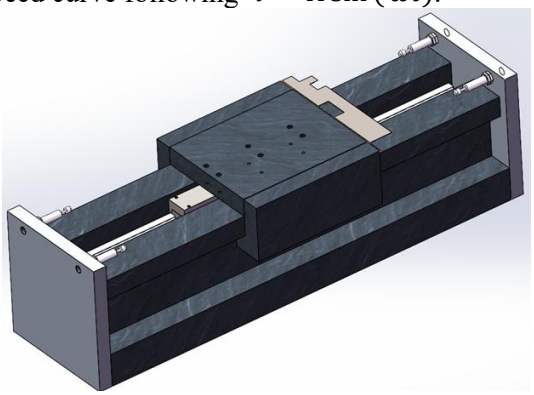

Figure 3. Simplified Vibration Table Assembly Model

The simulation analysis establishes two types of operating conditions: ideal conditions (neglecting gravitational effects and only considering Z-direction motion) and actual conditions (taking into account gravitational

loads and structural deformation). By comparing the motion parameters of the reference point (the midpoint of the table surface) under both conditions, we can quantify the lateral error.

3. Simulation Parameter Configuration

3.1 Material Property Settings

The material and mechanical properties of the core components of the vibration table are detailed in Table 1. The marble (used for the base and table surface) exhibits high stiffness and low deformation characteristics. The 6061-T6 aluminum alloy (used for the end cap) offers a good balance of strength and lightweight design, while the combination of DT4A pure iron and N38 neodymium magnets meets the requirements for electromagnetic drive[6]. All material properties were imported from the Abaqus material library or custom-created to ensure consistency between simulation parameters and the actual structure.

Table 1. Material List for Core Components of the Vibration Table

Component No.	Name	Material	Key Mechanical Properties
VEC05-01	End Cap	6061 T6	Elastic Modulus: 69 GPa, Poisson's Ratio: 0.33, Density: 2700 kg/m³
VEC05-02	Base	Marble	Elastic Modulus: 80 GPa, Poisson's Ratio: 0.25, Density: 2710 kg/m³
VEC05-03	Magnetic Base	DT4A+N38 Neodymium Magnet	DT4A: Elastic Modulus: 210 GPa, Density: 7850 kg/m³
VEC05-04	Joint Mounting Plate	Q235	Elastic Modulus: 206 GPa, Poisson's Ratio: 0.30, Density: 7850 kg/m³
VEC05.01-1	Table surface	Marble	Same as Base Material Properties
VEC05.01-2	Side Plate of Table surface	Marble	Same as Base Material Properties
VEC05.01-3	Magnetic Core	DT4A + Copper Wire	DT4A: Elastic Modulus: 210 GPa, Density: 7850 kg/m³

3.2 Assembly Constraints and Contact Settings

Based on the actual working conditions of the vibration table, two types of constraint relationships were established:

(1) Fixed Constraints: Components such as the end cap and the side of the base, the magnetic base and the base, and the table surface and the side plates were set with "bonded" constraints to simulate rigid connections.

(2) Contact Constraints: The bottom of the table surface and the top surface of the base are set for air bearing guideway contact. Referring to research by Liu Wei et al. [7], which indicates a friction coefficient of approximately 0.0005 (negligible), the simulation only defines the contact properties without specifying additional friction forces. The contact type is set as "Surface-Surface Contact (Standard)", as shown in Figure 4.

3.3 Analysis Steps and Load Settings

3.3.1 Planning of analysis steps

Seventeen characteristic frequency points were chosen at 1/3 octave intervals (0.1 Hz, 0.2 Hz, 0.5 Hz, 1 Hz, 2 Hz, 5 Hz, 10 Hz, 20 Hz, 31.5 Hz, 40 Hz, 50 Hz, 63 Hz, 80 Hz, 100 Hz, 125 Hz, 160 Hz, 200 Hz). Each frequency corresponds to an independent analysis step, with the duration of each analysis step set to one cycle of that frequency (T = 1/f). The setup interface is illustrated in Figure 5, ensuring the complete capture of vibrational responses.

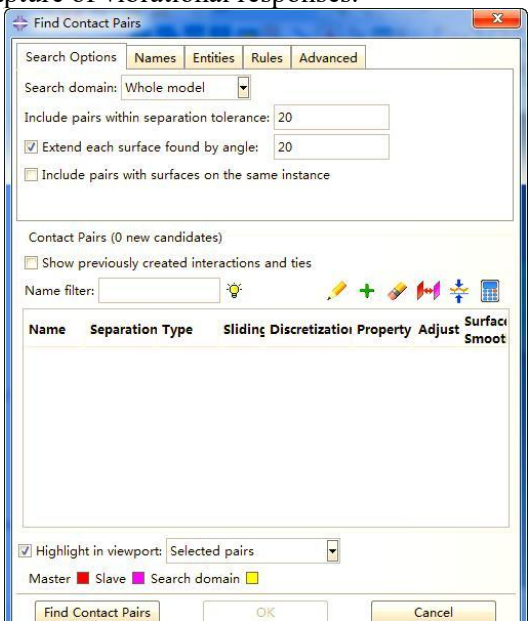

Figure 4. Interaction Settings for Contact Surface between Table Surface and Base

3.3.2 Load and boundary conditions

(1) Velocity Constraint: The table surface

undergoes sinusoidal motion along the Z direction, described by the velocity function v = $v = A\sin(\omega t)$, where $\omega = 2\pi f$. The amplitude A is determined by integrating the stroke (0.5 m) and is calculated as $A = \frac{0.5}{\pi}$. The corresponding parameters for different frequencies are shown in Table 2.

(2) Gravitational Load: A global gravitational acceleration (g = -9.8m/s²) is applied to the entire model in the negative Y direction to simulate the effect of actual gravity.

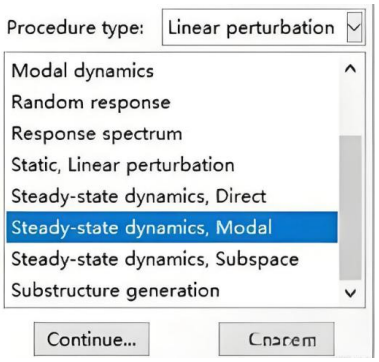

Figure 5. Analysis Step Setup

Table 2. Parameters for Velocity Relationships at Different Frequencies

Analysis Step	Frequency f (Hz)	Period T (s)	Angular Frequency ω (rad/s)	Amplitude A (m/s)	Output Frequency (every n increments)
1	0.1	10	0.628	0.157	n=1
2	0.2	5	1.257	0.314	n=1
3	0.5	2	3.142	0.785	n=1
4	1	1	6.283	1.571	n=1
5	2	0.5	12.566	3.142	n=1
6	5	0.2	31.416	7.854	n=1
7	10	0.1	62.832	15.708	n=1
8	20	0.05	125.664	31.416	n=1
9	31.5	0.0317	197.920	49.480	n=1
10	40	0.025	251.327	62.832	n=1
11	50	0.02	314.159	78.540	n=1
12	63	0.0159	395.841	98.960	n=1
13	80	0.0125	502.655	125.664	n=1
14	100	0.01	628.319	157.080	n=1
15	125	0.008	785.398	196.350	n=1
16	160	0.00625	1005.310	251.327	n=1
17	200	0.005	1256.637	314.159	n=1

3.4 Mesh Division

A combined mesh division strategy utilizing structured and unstructured grids was implemented. For regular components such as the base and table surface, hexahedral structured meshes were used. Conversely, for complex parts like the magnetic core and junction mounting plates, tetrahedral unstructured meshes were employed. The mesh size was controlled to be between 5 mm and 10 mm, ensuring a balance between computational accuracy and efficiency. The resulting mesh of the assembled model is shown in Figure 6, with a total element count of approximately 8.6×10^4 and a node count of around 1.2×10^5.

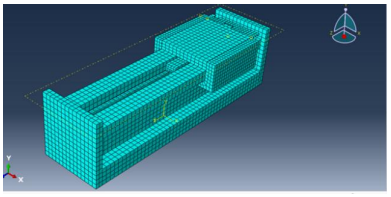

Figure 6. Mesh Division Results for the Vibration Table Assembly

4. Simulation Results and Analysis

4.1 Dynamic Characteristics under Ideal Conditions

In ideal conditions, the displacement of the reference point (the midpoint of the work platform) along the Z-axis demonstrates an ideal sinusoidal curve across various vibration frequencies. This is illustrated in Figure 7:

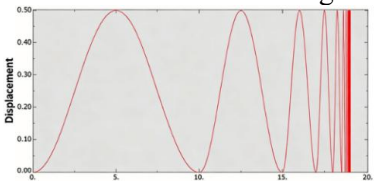

(a) Displacement curve for f = 0.1 to 200 Hz

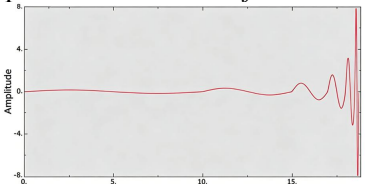

(b) Velocity curve for the reference point at f = 0.1 to 5 Hz

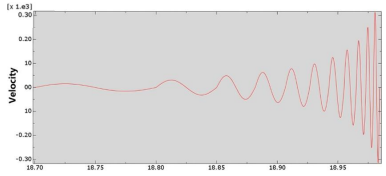

(c) Velocity curve for the reference point at f = 10 to 200 Hz

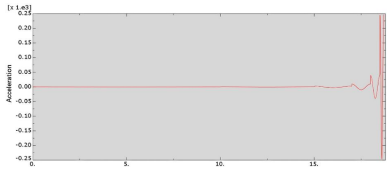

(d) Acceleration curve for the reference point at f = 0.1 to 5 Hz

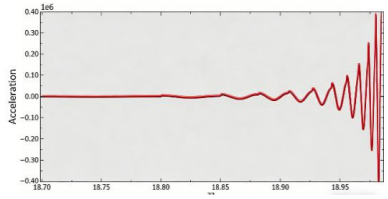

(e) Acceleration curve for the reference point at f = 10 to 200 Hz

Figure 7. Output Curves for Z-axis Displacement, Velocity, and Acceleration under Ideal Conditions

4.2 Lateral Displacement Characteristics under Gravity Influence

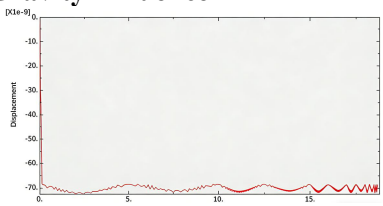

(a) Displacement curve for the reference point at f = 0.1 to 5 Hz

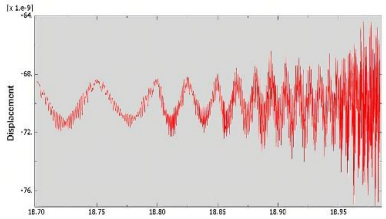

(b) Displacement curve for the reference point at f = 10 to 200 Hz

Figure 8. Simulation Results of Y-Direction Displacement Considering Gravity Influence

Under actual operating conditions, the guide rail experiences lateral displacement in the Y-direction due to bending from gravitational forces[7-8]. The displacement curve is shown in Figure 8. Since the gravitational load is applied at the initial moment of the analysis step, the reference point of the work platform has an initial Y-direction displacement of approximately -6.85×10^{-8} m. Therefore, the actual lateral displacement during the subsequent vibration process must account for this initial value.

The quantified results of the maximum Y-direction displacement at different frequencies for the reference point on the work platform are shown in Table 3. It can be observed that as the frequency increases, the maximum Y-direction displacement exhibits a gradual increase trend, rising from -3.36×10^{-9} m at 0.1 Hz to 8.54×10^{-9} m at 200 Hz. However, the overall displacements remain in the order of 10^{-9} m, indicating that the magnitude of displacement is extremely small[9].

Table 3. Maximum Y-Direction Displacement of the Reference Point at Different Frequencies

Frequency f/Hz	Maximum Y-direction Displacement /m (Negative values indicate Y-negative direction)	Relative Error (Compared to Z-direction Peak Displacement)
0.1	-3.36×10^{-9}	1.34×10^{-6}%
0.2	-3.48×10^{-9}	1.39×10^{-6}%
0.5	-3.49×10^{-9}	1.40×10^{-6}%
1	-3.49×10^{-9}	1.40×10^{-6}%
2	-3.50×10^{-9}	1.40×10^{-6}%
5	-3.50×10^{-9}	1.40×10^{-6}%
10	-3.50×10^{-9}	1.40×10^{-6}%
20	-3.77×10^{-9}	1.51×10^{-6}%
31.5	-3.92×10^{-9}	1.57×10^{-6}%
40	-4.85×10^{-9}	1.94×10^{-6}%
50	-5.02×10^{-9}	2.01×10^{-6}%
63	-5.49×10^{-9}	2.20×10^{-6}%
80	-6.20×10^{-9}	2.48×10^{-6}%
100	-6.69×10^{-9}	2.68×10^{-6}%
125	-7.11×10^{-9}	2.84×10^{-6}%
160	-7.81×10^{-9}	3.12×10^{-6}%
200	-8.54×10^{-9}	3.42×10^{-6}%

4.3 Quantitative Assessment of Error Influence

Based on the data presented in Table 3, we further calculated the bending angle of the guide rail, denoted as $\boldsymbol{\alpha}$ (where $\boldsymbol{\alpha} \approx \frac{\Delta Y}{L}$, with L being the effective length of the rail). The results show that the maximum bending angle is less than 0.000002∘, which corresponds to an additional acceleration error $\boldsymbol{a_{p,G} = g_{loc} \cdot \alpha}$ of approximately 3.33×10^{-10} m/s². This value is significantly lower than the peak acceleration values in the Z-direction (about 0.062 m/s² at 0.1 Hz and around 1.26×10^{5} m/s² at 200 Hz).

From an engineering application perspective, the relative error corresponding to the lateral displacement (compared to the Z-direction peak displacement) is a maximum of only 3.42×10^{-6}%. This level is entirely within the negligible range and will not have a substantial impact on the calibration accuracy of the visual vibration measurement system[10]. These results validate the rationality of the vibration table's structural design, indicating that there is no need to introduce additional correction models for compensation[11].

5. Conclusion

This study addresses the issue of lateral errors in low-frequency large displacement standard vibration tables, establishing a comprehensive analytical framework from theoretical modeling to simulation validation. The core conclusions are as follows:

A theoretical calculation model was proposed to describe the lateral errors caused by rail bending, clarifying the correlation mechanism between gravitational load and lateral displacement. This provides a theoretical basis for error analysis.

A refined simulation model consistent with the actual structure was developed, covering the full frequency range from 0.1 Hz to 200 Hz. The simulation process meets standardized requirements for error analysis in high-precision vibration equipment.

Quantitative results indicate that the maximum lateral error is 8.54×10^{-9} m, with a relative error of less than 3.5×10^{-6} %. The impact on measurement results is negligible, validating the reliability of the vibration table's structural design

The method developed in this study—comprising "structural simplification, parameter configuration, multi-frequency simulation, and error quantification"—can serve as a reference for error analysis in similar high-precision vibration equipment.

Future research could further consider factors such as temperature variations and material nonlinearities affecting errors, and refine simulation models using experimental data to enhance the comprehensiveness and accuracy of error analysis.

References

[1] Chen Xiaofeng, Wang Jianguo, Li Na. Application Research of Visual Vibrometry Technology in Noise Field Calibration of Civil Aircraft. Acta Aeronautica et Astronautica Sinica, 2023, 44(5): 321-330.

[2] Li Ming, Wang Qiang, Zhang Wei. Research Progress on Calibration Technology of Visual Vibrometry Systems. Journal of Instrumentation, 2022, 43(8): 1-18.

[3] Zhang Xuzhong, Liu Min, Chen Liang. Bending Error Analysis of Long-Travel Air Bearing Guideways. Journal of Mechanical Engineering, 2021, 57(12): 203-210.

[4] Zhao Haiyang, Li Gang, Wang Li. Characteristics and Suppression Methods of Bending Errors in Air Bearing Guideways. Journal of Mechanical Engineering, 2022, 58(10): 211-218.

[5] Liu Qiang, Zhang Min, Wu Hao. High-Precision Vibration Table Structural Simulation and Optimization Based on Abaqus. Vibration and Shock, 2022, 41(18): 167-173.

[6] Wang Lei, Zhao Yang, Sun Wei. Progress in Performance Testing and Error Compensation Technology of Vibration Tables. Journal of Instrumentation, 2023, 44(7): 89-98.

[7] Liu Wei, Zhang Ming, Li Juan. The design and research of aerostatic guideways performance testing bench. Acta Aeronautica et Astronautica Sinica, 2022, 43(3): 456-465.

[8] Wang Y, Li H, Zhang S. Simulation analysis of lateral error for low-frequency large-displacement vibration table. Journal of Vibration and Control, 2023, 29 (11-12): 2890-2899.

[9] Chen Gang, Zhao Wei, Wu Di. Structural Deformation Simulation Study of Vibration Tables Based on Abaqus. Vibration and Shock, 2021, 40(6): 156-161.

[10] Zhang Yi, Li Meng, Wang Hao. Experimental Verification and Simulation Correction of Lateral Errors of Low-Frequency Large-Displacement Air Bearing Guideway Vibration Tables. Journal of Metrology, 2023, 44(9): 1245-1253.

[11] Li Jun, Wang Fang, Zhang Hao. Cross-Section Optimization and Lateral Bending Error Suppression of Long-Travel Vibration Table Guideways. Aviation Precision Manufacturing Technology, 2024, 60(2): 56-63.